Detection of Echoes Using Time-Frequency Analysis Techniques

Pasquale Daponte, *Member, IEEE*, Giuseppe Fazio, and Anna Molinaro

Abstract— **The following is a presentation of echo detection techniques based on time-frequency signal analysis for the measuring of thickness in thin multilayer structures. These techniques are shown to provide high-resolution signal characterization in a time-frequency space, and good noise rejection performance. In particular, the Short-Time Fourier Transform, the Gabor expansion, the Cross-Ambiguity Function and the Wigner-Ville Distribution are analyzed and compared with techniques such as the logarithmic power spectrum, Cepstrum and the Segmented Chirp Z-Transform. A suitable operating procedure was set up, based on an initial emulation phase in which simulated signals were considered, followed by a second phase in which real signals were processed. The results show the optimum performances of these new techniques compared with the traditional ones and, in particular, that the accurate measurement of thickness can be obtained also when waveform transients partially overlap.**

I. Introduction

DIGITAL signal processing is being increasingly utilized in different fields, because of the increased availability of equipment which has both a high data acquisition capability and is capable of performing complex computations of the sampled data in a short time. In particular, the setting up of suitable computational techniques is indispensable, for signals in noisy environments, to the extraction of the required information from the signal [1]–[3]. This is the case for ultrasonic signals, especially when used to measure thin thicknesses of multilayer structures. In order to obtain accurate measurements of these types of thicknesses, a suitable processing of the echoes from the structure under analysis is required [2]–[5].

The analysis can be performed directly in the time domain but, unfortunately, the attenuation of higher frequencies and the dispersive nature of the waves cause the individual echoes to change shape and to overlap which makes the estimation of the echoes' arrival times difficult. To overcome these limits, some methods, based on deconvolution algorithms, have been proposed. They are, however, very noise sensitive [3]–[5] and, consequently, unsuitable for detecting echoes from thin multilayer structures in noisy environments.

Better performances can be achieved by operating in the frequency domain, and possible approaches are based on the evaluation of the ultrasonic signal under test by means of (i) the logarithmic power spectrum (LogFFT) [6]–[8], (ii) the Cepstrum [4], and (iii) the Segmented Chirp Z-Transform (SCZT) together with a flexible window [2]. However, these methods also fail for very low signal-to-noise ratios (SNR) and/or for a very low number of samples of the signal under test. In fact, the theory underlying all these traditional methods is based on the assumption that the ultrasonic signals are stationary, but the nonstationary nature of these signals is evident and results from variations of the propagation media, channel characteristic variations, nonlinear modulation and so on. For this reason, the authors propose a new approach to the measuring of thin thicknesses in noisy environments, based on ultrasonic signal representations that use both time and frequency as independent variables.

Time-Frequency Representations (TFR's) map a one-dimensional signal of time, $x(t)$, onto a two-dimensional function of time and frequency, $T_X(t, f)$. Most TFR's are "time-varying spectral representations" which are conceptually similar to a musical score with time running along one axis and frequency along the other. The values of the TFR surface above the time-frequency plane give an indication as to which spectral components are present at which times [9]–[12].

In this paper, the authors analyze TFR performances, with reference to their noise rejection in thickness measurement in thin multilayer structures. To carry out performance analysis, an operating procedure, based on a previous emulation phase in which the implemented algorithms were applied to simulated signals in noisy environments, was established. This emulation phase is essential since it allows the algorithm to operate on signals with known characteristics, thereby permitting their correctness to be evaluated. The algorithms were then applied to the ultrasonic signals returning from real multilayer structures.

All the experimental results, both for simulated and real signals, pertain to the field of ophthalmic echography [13]. This represents a significant application area because both thin structures (100 μm thicknesses) and noticeable noise sources are present in the eye [14]. By noise sources, we mean both "measurement noise" and "in vivo operation process noises". The former is due to the echograph (pulser, transducer, and receiver) and to the data acquisition system (input amplifier and A/D converter) [15]–[16]; the latter is due to the non-perpendicularity between the tissue and the ultrasound beam and to tissue inhomogeneity [17]. Other problems may arise from incorrect synchronization of the echograph and the data acquisition system as well as from the computational process.

II. Algorithms Used for Signal Elaboration

In what follows, the algorithms used to improve the detectability of echoes in noisy environments are briefly described in order to highlight their peculiarities when used in the

Manuscript received June 2, 1994; revised December 15, 1994.

P. Daponte is with the Department of Computer Science and Electrical Engineering, University of Salerno, 84084 Fisciano (SA), Italy.

G. Fazio and A. Molinaro are with the Department of Electronic Computer and System Science, University of Calabria, 87030 Rende CS, Italy.

Publisher Item Identifier S 0018-9456(96)00046-0.

0018–9456/96$05.00 © 1996 IEEE

Authorized licensed use limited to: Columbia University. Downloaded on February 8, 2009 at 20:43 from IEEE Xplore. Restrictions apply.

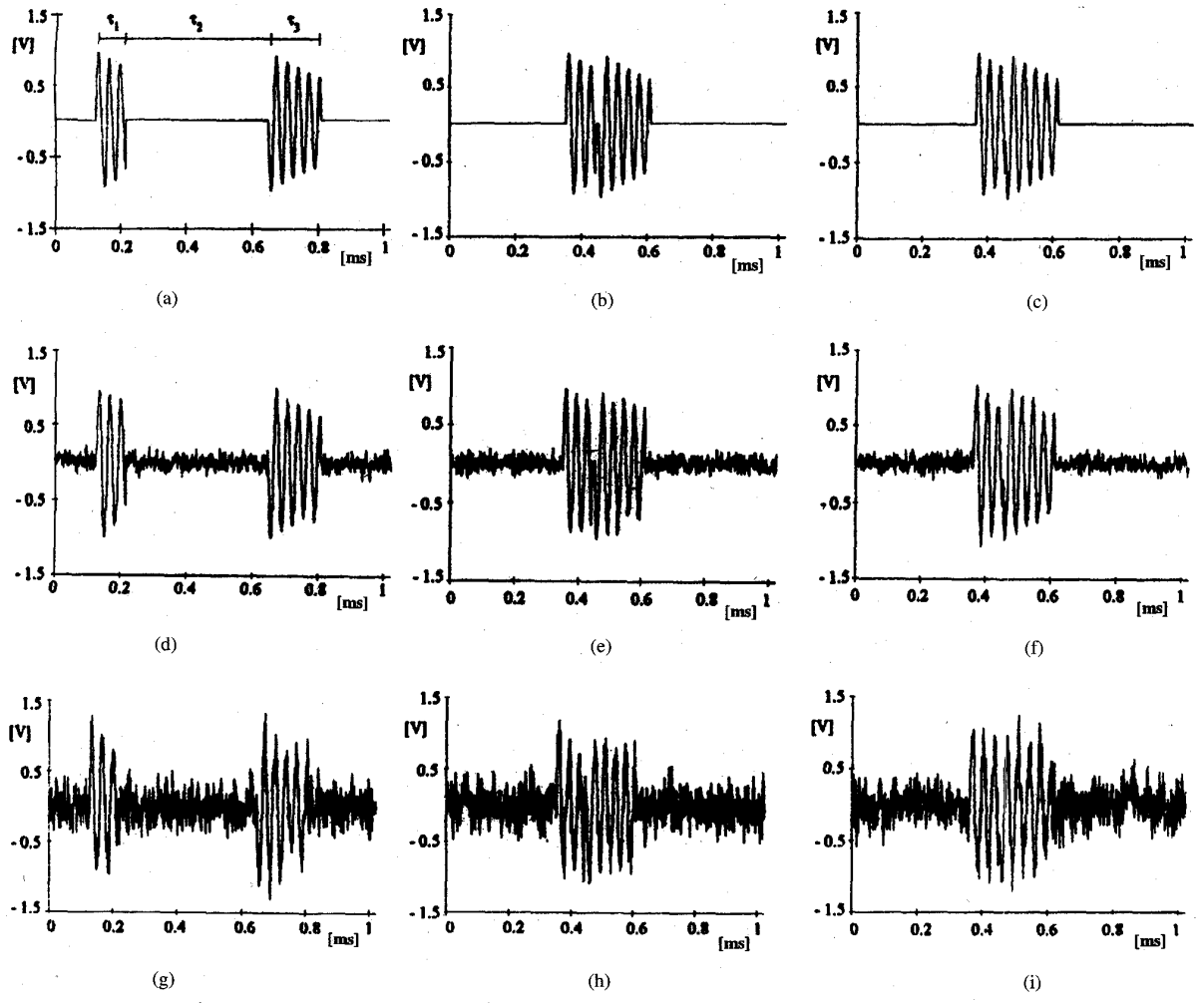

Fig. 1. Simulated signal consisting of two sinusoidal bursts: (a) SNR $= \infty$, $\tau_1 = 70$ μs, $\tau_2 = 451$ μs, $\tau_3 = 160$ μs; (b) SNR $= \infty, \tau_1 = 70$ μs, $\tau_2 = 21$ μs, $\tau_3 = 160$ μs; (c) SNR $= \infty, \tau_1 = 70$ μs, $\tau_2 = 1$ μs, $\tau_3 = 160$ μs,; (d) SNR $= 20$ dB, $\tau_1 = 70$ μs, $\tau_2 = 451$ μs; $\tau_3 = 160$ μs; (e) SNR $= 20$ dB, $\tau_1 = 70$ μs, $\tau_2 = 21$ μs, $\tau_3 = 160$ μs; (f) SNR $= 20$ dB, $\tau_1 = 70$ μs, $\tau_2 = 1$ μs, $\tau_3 = 160$ μs; (g) SNR $= 5$ dB, $\tau_1 = 70$ μs, $\tau_2 = 451$ μs, $\tau_3 = 160$ μs; (h) SNR $= 5$ dB, $\tau_1 = 70$ μs, $\tau_2 = 21$ μs, $\tau_3 = 160$ μs; (i) SNR $= 5$ dB, $\tau_1 = 70$ μs, $\tau_2 = 1$ μs, $\tau_3 = 160$ μs.

presence of noise. In particular, this section first discusses linear TFR's, concentrating on the Short-Time Fourier Transform (STFT), Gabor expansion, and the Cross-Ambiguity Function (CAF) and, second, a quadratic TFR, concentrating on the Wigner-Ville Distribution (WVD).

A. Short-Time Fourier Transform

The Fourier Transform (FT) and its inverse establish a one-to-one relationship between the time domain (signal $x(t)$) and the frequency domain (spectrum $X(f)$). The time domain and frequency domain constitute two alternative ways of looking at a signal. Although the FT allows a passage from one domain to the other, it does not allow a combination of the two domains. In particular, information about time is not easily accessible in the frequency domain. While the spectrum $X(f)$ shows the overall strength with which any frequency f is contained in the signal $x(t)$, it does not generally provide easy-to-interpret information about the time localization of spectral components [9]–[12], [18].

Although the FT (spectrum) does not explicity show the time localization of frequency components, such a time localization can be obtained by suitable prewindowing of the signal $x(t)$. Accordingly, the *Short-Time Fourier Transform* (STFT) or short-time spectrum, of a signal $x(t)$ is defined as

$$\mathrm{STFT}_x^{(\gamma)}(t,f) = \int_{-\infty}^{\infty} [x(t')\gamma^*(t'-t)]e^{-j2\pi ft'}\,dt'. \quad (1)$$

The STFT at time t is the FT of the signal $x(t')$ multiplied by a shifted "analysis window" $(t'-t)$ centered around t. (The superscript * denotes complex conjugation). Because multiplication by the relatively short window $^*(t'-t)$ effectively suppresses the signal outside the neighborhood of the analysis time point $t' = t$, the STFT is simply a "local spectrum" of the signal $x(t')$ around the "analysis time" t [9].

The STFT is a linear TFR. That is, it depends linearly upon the signal $x(t)$. Moreover, the STFT result $\mathrm{STFT}_x^{(\gamma)}(t,f)$ for a given signal $x(t')$ is significantly influenced by choice of the analysis window $^*(t'-t)$. The STFT may also be expressed

Authorized licensed use limited to: Columbia University. Downloaded on February 8, 2009 at 20:43 from IEEE Xplore. Restrictions apply.

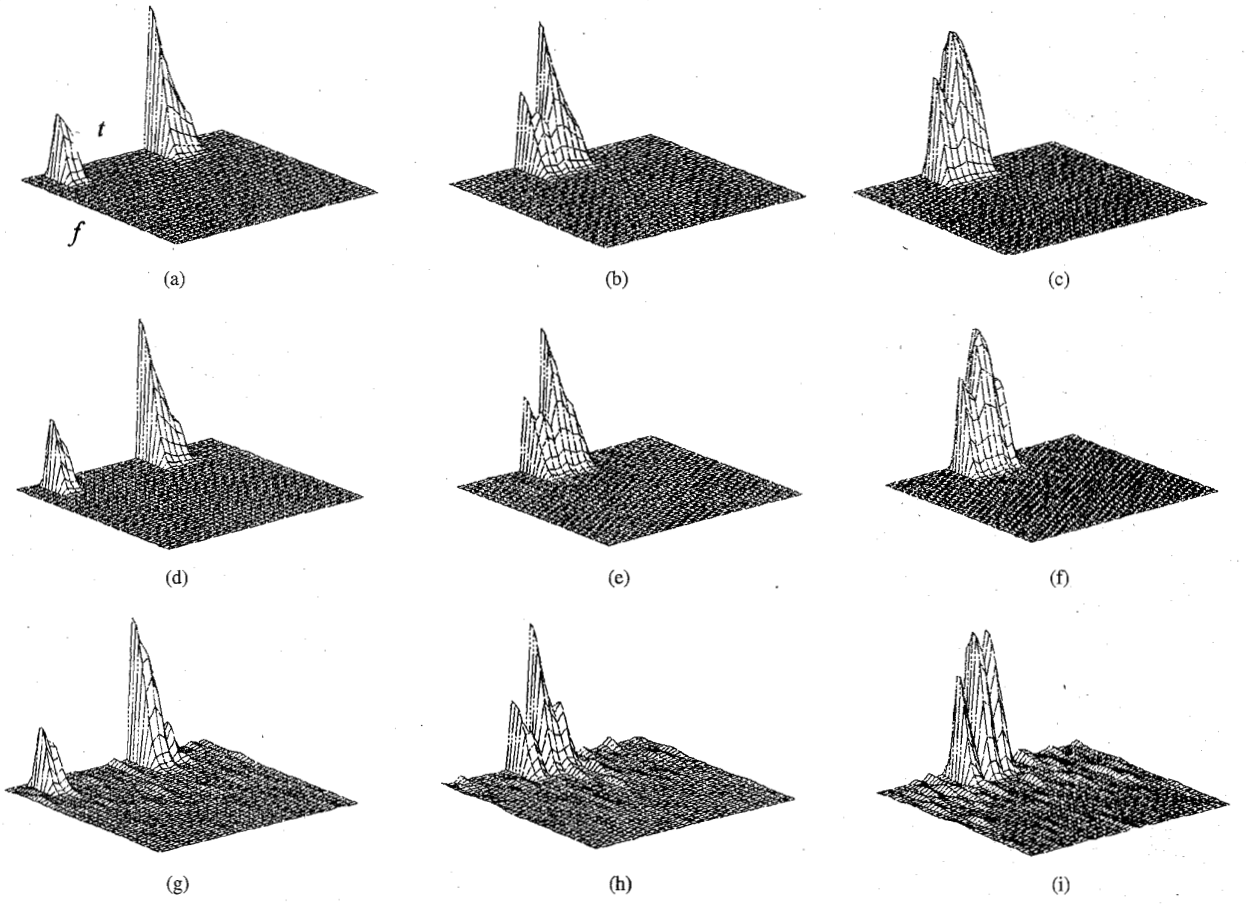

Fig. 2. STFT application to the simulated signals of Fig. 1(a)–(i).

in terms of the signal and window spectra [9]

$$\mathrm{STFT}_x^{(\gamma)}(t,f) = e^{-j2\pi tf} \int_{f'} X(f')\Gamma^*(f'-f)e^{j2\pi tf'}\,df'. \quad (2)$$

Apart from the phase factor $e^{-j2\pi tf'}$, this "frequency-domain expression" is analogous to the time-domain expression (1). In fact, it shows that the STFT can also be interpreted as the inverse FT of the "windowed spectrum", $X(f')\Gamma^*(f'-f)$, in which the spectral window $\Gamma(f)$ is simply the FT of the temporal window (t).

For practical application of the STFT, it is necessary to discretize the time-frequency plane. We therefore consider samples of the STFT at equidistant time-frequency grid points (nT, kF) where $T > 0$ and $F > 0$ are the sampling periods for the time and frequency variables, respectively, and n and k are integers

$$\mathrm{STFT}_x^{(\gamma)}(nT,kF) = \int_{t'} x(t')\gamma^*(t'-nT)e^{-j2\pi kFt'}\,dt'.$$

B. Gabor Representation

A Gabor representation of a signal $x(t)$ is a series expansion of the form [19]–[24]

$$x(t) = \sum_{m=-\infty}^{+\infty} \sum_{n=-\infty}^{+\infty} a_{m,n} w(t-nT)e^{(j2\pi mt/T)} \quad (3)$$

The terms of this expansion are (i) a set of complex weights $\{a_{m,n}$ with m, n positive integers$\}$ called the *Gabor coefficients*, and (ii) a set of time and frequency translations of a single function, $w(t)$, the *window*. The translations of $w(t)$ form the Gabor basis $\{w_{m,n}(t)\}$ as

$$w_{m,n}(t) = w(t-nT)e^{(j2\pi mt/T)} \quad (4)$$

with m and n being positive integers.

The grid of time-frequency points, $(t_n, f_m) = (nT, m/T)$, over which $w(t)$ is displaced in forming $\{w_{m,n}(t)\}$—called the *von Neumann* or *Gabor lattice*—defines a unit area cell of dimension $T \cdot (1/T)$ in the time-frequency plane.

In (3) we have a synthesis formula which tells how to recover a function from its expansion coefficients. There is a corresponding need for analysis formulae that generate those coefficients $a_{m,n}$ from the data signal. We investigate two rather different looking analytic means of computing the Gabor transform, given the window function and the von Neumann grid: the biorthogonal method and the Zak transform method.

The Biorthogonal Method: In the biorthogonal method, both the basis functions $\{w_{m,n}(t)\}$ and a related set of biorthogonal functions $\{b_{m,n}(t)\}$ [19] are used

$$b_{m,n}(t) = b(t-nT)e^{(j2\pi mt/T)} \quad (5)$$

Authorized licensed use limited to: Columbia University. Downloaded on February 8, 2009 at 20:43 from IEEE Xplore. Restrictions apply.

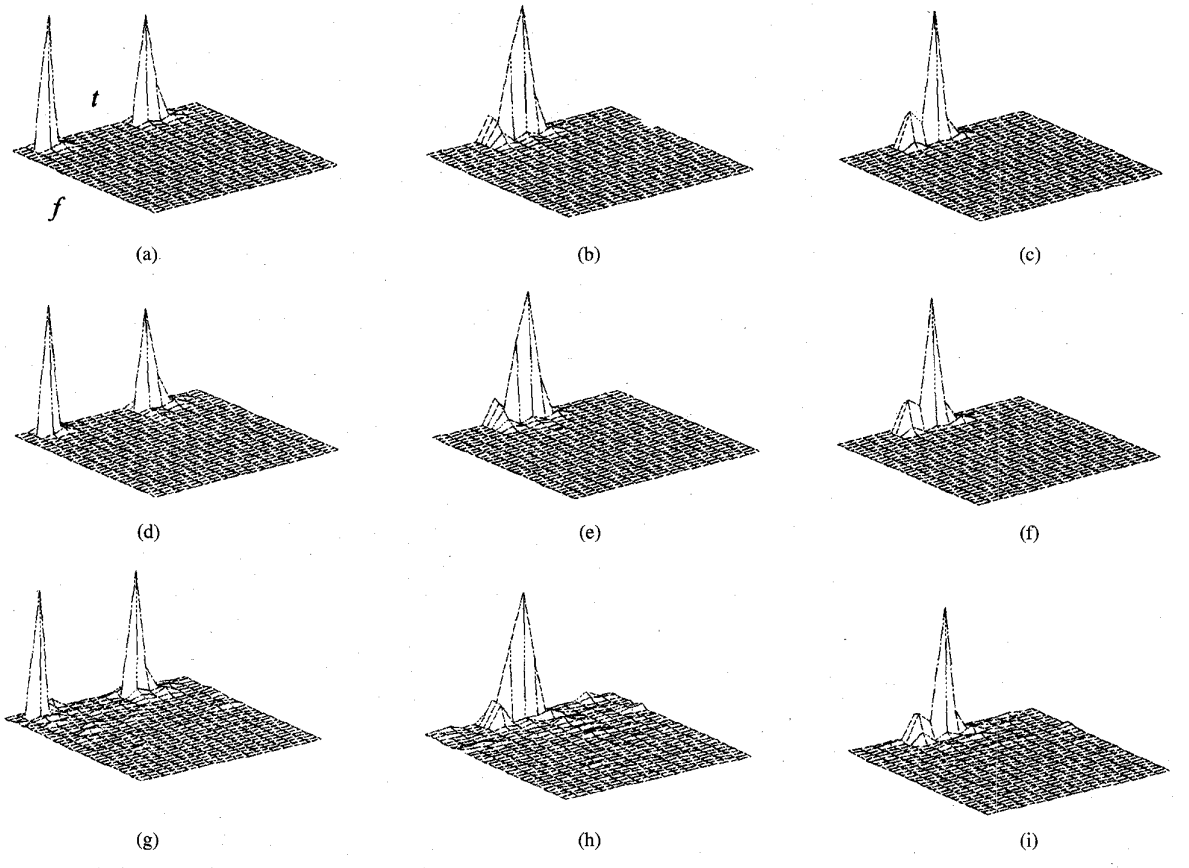

Fig. 3. Results obtained by using the Gabor representation applied to simulated signals of Fig. 1(a)–(i). The coefficients $a_{m,n}$ are computed by means of the biorthogonal method.

with m and n being positive integers, and the terms $b_{m,n}(t)$ generated from a function $b(t)$ having the property

$$\langle w_{m,n} \mid b_{p,q} \rangle = \int_{-\infty}^{+\infty} w(t - nT) b^*(t - qT) \cdot e^{[j2\pi(m-p)t/T]}\, dt = \delta_{n-q}\delta_{m-p} \tag{6}$$

where $\langle\rangle$ is the inner product and δ is the delta-Dirac.

If such a $b(t)$ exists, (6) permits analysis of $x(t)$ into its coefficients by the inner products of $x(t)$ and $\{b_{m,n}(t)\}$ according to the formula

$$a_{m,n} = \langle x \mid b_{m,n} \rangle = \int_{-\infty}^{+\infty} x(t) b^*_{m,n}(t)\, dt \tag{7}$$

as is shown by the development

$$\begin{aligned} \langle x \mid b_{m,n} \rangle &= \int_{-\infty}^{\infty} x(t) b^*_{m,n}(t)\, dt \\ &= \int_{-\infty}^{\infty} \sum_{p=-\infty}^{\infty} \sum_{q=-\infty}^{\infty} a_{p,q} w_{p,q}(t) b^*_{m,n}(t) \\ &= \sum_{p=-\infty}^{\infty} \sum_{q=-\infty}^{\infty} a_{p,q} \int_{-\infty}^{\infty} w_{p,q}(t) b^*_{m,n}(t) \\ &= \sum_{p=-\infty}^{\infty} \sum_{q=-\infty}^{\infty} a_{p,q} \delta_{m-p}\delta_{n-q} = a_{m,n}. \end{aligned} \tag{8}$$

The interchange of the integral and summations in (8) requires uniform convergence of the sum.

The Zak Transform Method: A second analysis formula is based upon the Zak transform [25], [26], a time-frequency mapping given by [19]

$$Z_X(\nu, \tau) = \sum_{k=-\infty}^{\infty} x(kT + \tau) e^{(-j2\pi k\nu T)}. \tag{9}$$

Interpretation of the Zak transform as a time-offset DFT will be useful in the sequel. Taking Zak transforms on both sides of (3) yields the following relation among the Zak transforms of X and w, and the Gabor coefficients

$$Z_X(\nu, \tau) = Z_w(\nu, \tau) \sum_{m=-\infty}^{\infty} \sum_{n=-\infty}^{\infty} a_{m,n} \cdot e^{[j2\pi(m\tau/T) - n\nu T]}. \tag{10}$$

The $\{a_{m,n}\}$ are found formally by inverting the two-dimensional Fourier series on the right

$$a_{m,n} = \int_0^T d\tau \int_0^{1/T} \frac{Z_X(\nu, \tau)}{Z_w(\nu, \tau)} \cdot e^{[j2\pi(-m\tau/T + n\nu T)]}\, d\nu. \tag{11}$$

C. Cross-Ambiguity Function

The Cross-Ambiguity Function of a signal $x(t)$ relative to a reference signal $g(t)$ is defined by the formula [9]–[12], [27]

Authorized licensed use limited to: Columbia University. Downloaded on February 8, 2009 at 20:43 from IEEE Xplore. Restrictions apply.

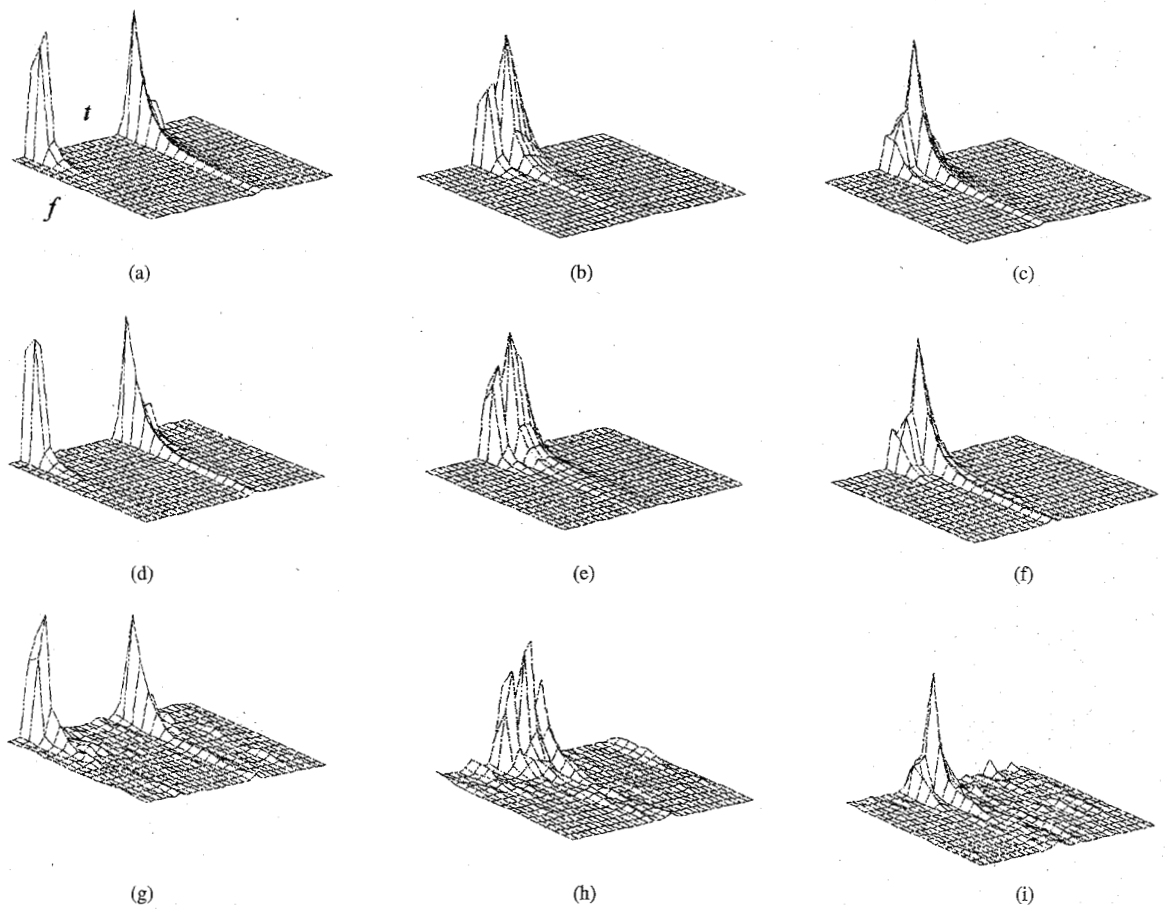

Fig. 4. Results obtained by using the Gabor representation applied to simulated signals of Fig. 1(a)–(i). The Zak transform is used to compute the coefficients $a_{m,n}$.

$$\mathrm{CAF}(x,g)(u,v) = \int_{-\infty}^{+\infty} x(t)g^*(t-\nu)e^{j2\pi ut}\,dt, \quad \text{with } u \text{ and } \nu \text{ real.} \tag{12}$$

We assume that both $x(t)$ and $g(t)$ have energy with $\|g\| > 0$, Setting

$$g_{u\nu}(t) = g(t-\nu)e^{-j2\pi ut} \tag{13}$$

we can rewrite (12) as

$$\mathrm{CAF}(x,g)(u,\nu) = \langle x, g_{u,\nu}\rangle. \tag{14}$$

The signal can be reconstructed, up to the factor $g^*(t-\nu)$, by the inversion formula

$$x(t)g^*(t-\nu) = \int_{-\infty}^{+\infty} \mathrm{CAF}(x,g)(u,\nu)e^{-j2\pi tu}\,du. \tag{15}$$

We will restrict the continuous parameters $(u,\nu) \in R^2$ to points on the lattice of R^2. Choose $a, b > 0$ and sample the Cross-Ambiguity Function at the points of the corresponding lattice

$$\mathrm{CAF}(x,g)((ma),(nb)) = \langle x, g_{(ma),(nb)}\rangle \quad \text{with } m \text{ and } n \text{ being integers.} \tag{16}$$

The signal in (16) can be implemented using the Zak transform [25], [26].

D. Wigner-Ville Distribution

For a continuous-time signal $x(t)$ the Wigner-Ville Distribution is defined as [9]–[12], [28]–[30]

$$D_x(t,f) = \int_{-\infty}^{\infty} x\left(t+\frac{\tau}{2}\right)x^*\left(t-\frac{\tau}{2}\right)e^{[-j2\pi f\tau]}\,d\tau. \tag{17}$$

In the frequency domain, the corresponding definition is

$$D_x(t,f) = \int_{-\infty}^{\infty} X\left(f+\frac{\xi}{2}\right)X^*\left(f-\frac{\xi}{2}\right)e^{[-j2\pi f\xi]}\,d\xi. \tag{18}$$

Let $w(t)$ be a window function which satisfies $w(t) = 0$ for $|t| > \frac{T_w}{2}$ and $z(t)$ the analytical signal derived from $x(t)$, defined as

$$z(t) = x(t) + jH[x(t)] \tag{19}$$

where $H[x(t)]$ is the Hilbert transform of $x(t)$, and the WV distribution is defined in the time domain as

$$D_x(t,f) = \int_{-Tw}^{Tw} z\left(t+\frac{\tau}{2}\right)z^*\left(t-\frac{\tau}{2}\right)w\left(\frac{\tau}{2}\right)w^*\left(-\frac{\tau}{2}\right)e^{[-j2\pi f\tau]}\,d\tau. \tag{20}$$

Authorized licensed use limited to: Columbia University. Downloaded on February 8, 2009 at 20:43 from IEEE Xplore. Restrictions apply.

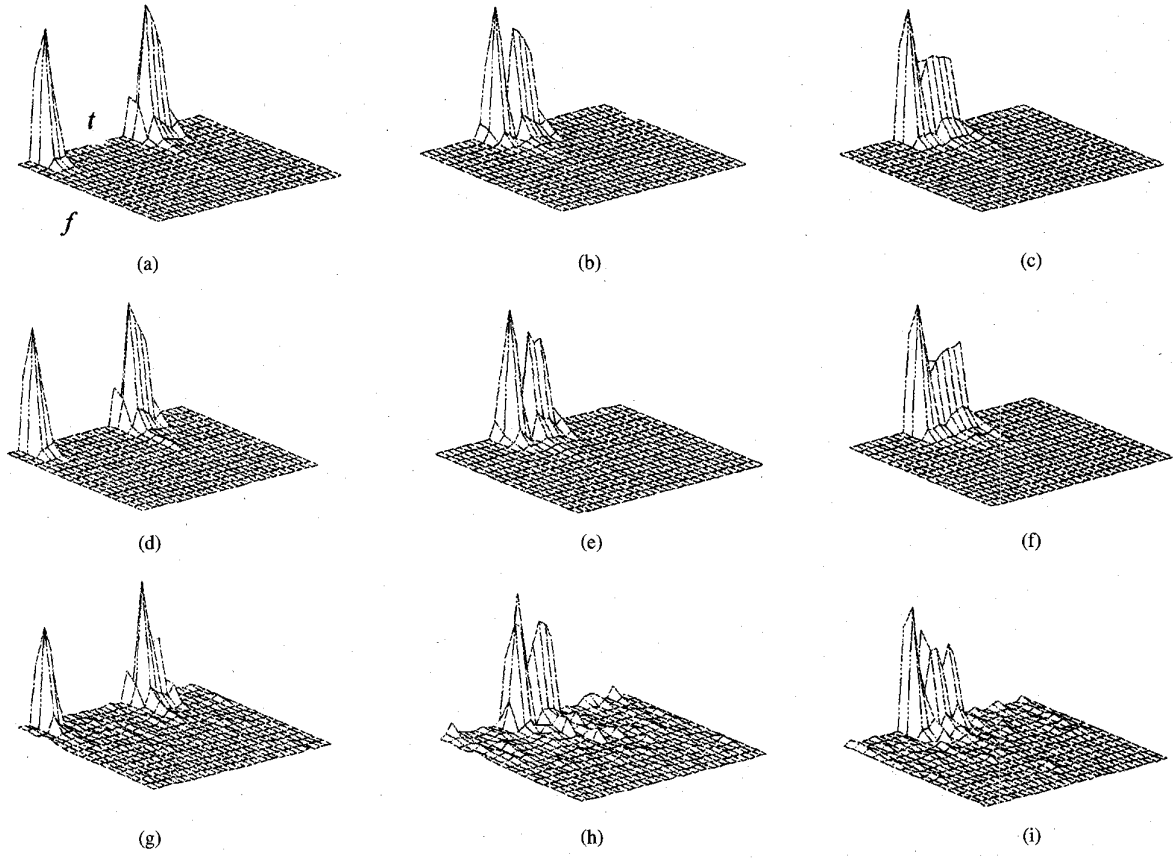

Fig. 5. CAF application to simulated signals of Fig. 1(a)–(i).

The discrete-time equivalent of (20) is

$$D_x(nT, f) = 2T \sum_{l=-L}^{L} z(nT + lT)z^*(nT - lT)w(l)w^*(-l)e^{[-j4\pi ft\tau]} \tag{21}$$

where T is the sampling period and $w(lT) = 0$, for $|l| > L$; L is a positive integer [28]–[37].

III. Operating Procedure and Experimental Results

The performance of the algorithms when measuring multilayer structure thicknesses cannot always be compared by applying the algorithms directly to real signals. If an ophthalmic thickness measurement is required, for example, the correctness of the algorithm set up for this purpose can be tested only by applying the algorithm to signals with known characteristics and similar to the actual one. Such an emulation phase also permits easy evaluation and optimization of algorithm noise rejection, thus allowing tests simulating different environmental conditions. Thus, an operating procedure based on a previous emulation phase was set up followed by the application of the proposed algorithms to real signals [2].

In order to emulate ultrasonic ophthalmic signals, the posterior surface of the human eye can be represented as a multilayer structure with three layers (retina, choroid, and sclera) [6], [8], [13]. The ultrasonic signal from this structure is composed of (i) a composite echo produced by interference between the echoes from the anterior and posterior surfaces of the retina; (ii) an echo caused by the boundary surface between the choroid and the sclera; and (iii) an echo from the posterior surface of the sclera. Choroid and sclera thicknesses, connected with echoes (i), (ii) and (iii), are large enough to be easily measured in the time domain. To obtain the retina thickness from the composite echo (i), however, requires more complex techniques to be set up. Hence, attention here is focused on an ultrasonic signal backscattered from a single layer, emulating the retina, modulated in both amplitude and phase. As a consequence the signal was simulated by means of a two-component signal $s(t) = s_1(t) + s_2(t)$ consisting of the sinusoidal bursts

$$s_1(t) = \begin{cases} A_1 e^{-k_1 t}\cos(2\pi ft + \varphi_1), & t_1 < t < t_2 \\ 0, & \text{otherwise} \end{cases} \tag{22}$$

and

$$s_2(t) = \begin{cases} A_2 e^{-k_2 t}\cos(2\pi ft + \varphi_2) & t_3 < t < t_4 \\ 0, & \text{otherwise.} \end{cases} \tag{23}$$

In particular, the algorithm performances can be investigated by varying noise amplitude and bandwidth as well as the signal characteristics connected with simulated layer thickness and acoustic impedance.

Authorized licensed use limited to: Columbia University. Downloaded on February 8, 2009 at 20:43 from IEEE Xplore. Restrictions apply.

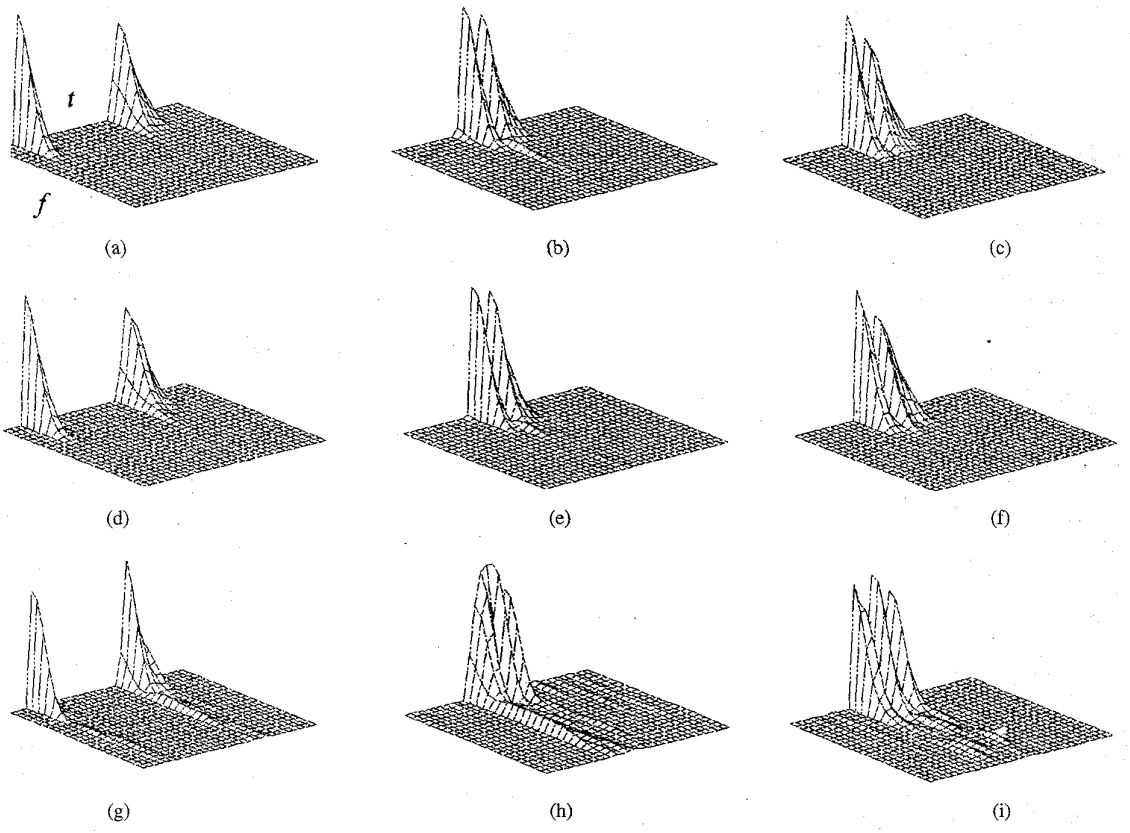

Fig. 6. WVD application to simulated signals of Fig. 1(a)–(i).

TABLE I
PARAMETER CHARACTERIZING THE TEST SIMULATED SIGNALS

Signal	t_1 [μs]	t_2 [μs]	t_3 [μs]	t_4 [μs]	A_1 [V]	A_2 [V]	φ_1 [°]	φ_2 [°]	f [kHz]	k_1	k_2
1	20	90	541	701	1	1	45	235	30	3000	3000
2	20	90	111	271	1	1	45	235	30	3000	3000
3	20	90	91	251	1	1	45	235	30	3000	3000

A. Tests on Simulated Signals

Fig. 1(a) shows a signal which simulates one from a layer with a thickness large enough to allow detection of the separation surfaces. In fact, the time interval $\tau_1 = (t_2 - t_1)$ represents the echo from the anterior surface, the time interval $\tau_3 = (t_4 - t_3)$ the echo from the posterior surface, and τ_2 the time interval between the two echoes. The second echo has been dephased with regard to the first one in order to simulate acoustic impedance variation. By varying the time interval τ_2 between the two echoes, several thicknesses can be simulated as is shown in Fig. 1(b) and (c). With reference to (22) and (23), the parameter values chosen are shown in Table I.

The signals of Fig. 1(a)–(c) were also contaminated with uniform noise, thus giving signals such as those shown in Fig. 1(d)–(f), with SNR = 20 dB and Fig. 1(g)–(i) with SNR = 5 dB. The sample number chosen was equal to 1024, and the sampling frequency equal to 1 MHz. The TFR's and traditional analysis techniques were applied to the test signals. For each noise and thickness condition, the simulations were repeated 100 times, and the mean $(\bar{x})$ and standard deviation (σ) on the position of the reflection were calculated and given in Table II together with the number of ambiguity cases in the time interval measurement. A comparison of the obtained results highlights the following.

- The STFT (Fig. 2(a)–(i)), with the Hamming window as analysis window $\gamma(t' - t)$, allows echo detection also in the presence of noise, but when waveform transients partially overlap and the noise increases (Fig. 2(h) and (i)), ambiguity in the echo classification arises. In fact, in Fig. 2(h) and (i) a third echo, not corresponding to the structure of the simulated signal, is shown.
- The Gabor representation gives good results (Fig. 3(a)–(i)) when the biorthogonal method is used to compute the coefficients $a_{m,n}$. In particular, according to [20] the same procedure has been used choosing $\lambda = 1, L = 64$ and $N = 16$ (cfr. Eqs. (17) and (18)

Authorized licensed use limited to: Columbia University. Downloaded on February 8, 2009 at 20:43 from IEEE Xplore. Restrictions apply.

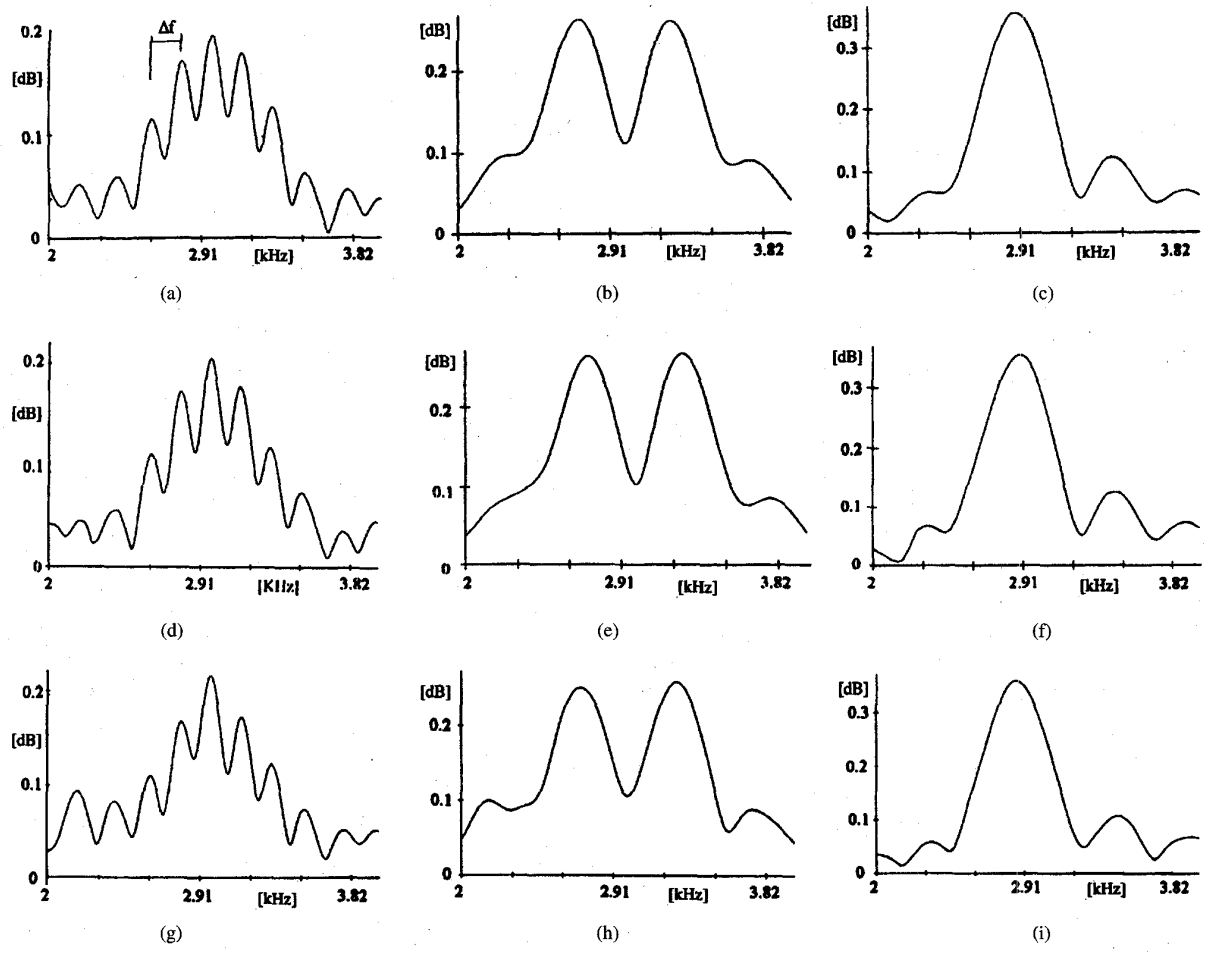

Fig. 7. Application of the SCZT to the simulated signals of Fig. 1(a)–(i).

TABLE II
MEAN ($\bar{x}$), STANDARD DEVIATION (σ) AND AMBIGUITY CASES [%] IN ECHO DETECTION VERSUS ALGORITHM

	SNR=20dB									SNR=5dB								
	$\tau_1+\tau_2$=521μs			$\tau_1+\tau_2$=91μs			$\tau_1+\tau_2$=71μs			$\tau_1+\tau_2$=521μs			$\tau_1+\tau_2$=91μs			$\tau_1+\tau_2$=71μs		
	$\bar{x}$[μs]	σ[μs]	[%]	$\bar{x}$[μs]	σ[μs]	[%]	$\bar{x}$[μs]	σ[μs]	[%]	$\bar{x}$[μs]	σ[μs]	[%]	$\bar{x}$[μs]	σ[μs]	[%]	$\bar{x}$[μs]	σ[μs]	[%]
STFT	509	8	7	101	12	18	66	12	20	502	14	19	106	15	34	68	16	38
GABOR(1)	510	7	0	98	8	0	70	18	0	509	8	0	98	8	5	70	19	10
GABOR(2)	508	10	0	100	11	0	75	18	38	508	10	2	99	10	17	76	21	58
CAF	510	7	0	110	16	14	74	23	49	509	9	0	101	12	37	76	23	68
WVD	510	7	3	98	8	7	70	19	8	509	8	11	99	9	17	72	27	25

(1)Biorthogonal method (2)Zak Transform

in [20]). In this case, echo detection is both possible and unambiguous also in the presence of noise and with partially overlapped echoes. Problems can arise in the estimation of the first coefficient, if it is very small when compared with the second.

- The worst results are obtained if the Zak transform is used to compute the coefficients $a_{m,n}$ (Fig. 4(a)–(i)). In this case, decreasing the time interval between the echoes causes a failure in echo detection, while increasing the noise causes ambiguities to appear in the echo detection.
- The CAF application, with the Hamming window as reference signal $g(t)$, on test signals produces unacceptable results (Fig. 5(a)–(i)). In particular, the second echo is not clearly detectable without noise also contaminating the simulated signals (Fig. 5(a)).
- The WVD, with the Hamming window, furnishes excellent results both in the presence of noise and with partially overlapped echoes (Fig. 6(a)–(i)). Only in Fig. 6(i) does a third coefficient not related to the simulated signals shown in Fig. 1(i) appear.

Authorized licensed use limited to: Columbia University. Downloaded on February 8, 2009 at 20:43 from IEEE Xplore. Restrictions apply.

TABLE III
MEAN ($\bar{x}$), STANDARD DEVIATION (σ) AND AMBIGUITY CASES [%] IN RETINA-CHOROID DETECTION VERSUS ALGORITHM

	Retina		Choroid		Ambiguity cases
	$\bar{x}$ [μm]	σ[μm]	$\bar{x}$ [μm]	σ[μm]	[%]
STFT	171	37	336	57	43
GABOR[1]	169	42	352	62	34
GABOR[2]	158	51	363	73	40
CAF	163	60	370	91	82
WVD	167	25	346	47	30
SCZT	140	11	-	-	-

(1)Biorthogonal method (2)Zak Transform

Where echo detection is possible all these TFR's give excellent results in terms of errors in the thickness measurement. These results can also be compared with those obtainable by traditional techniques.

1) Fig. 1(f)–(h) and (i) clearly highlight the fact that traditional techniques of directly measuring echo times cannot be applied in a noisy environment.
2) The Cepstrum technique and the logarithmic power spectrum, as shown in [2], fail to give accurate results when the SNR decreases. In particular, when it is possible to measure the frequency interval applying the logarithmic power spectrum technique, the estimated error in the thickness measurement is in the order of 20%.
3) The SCZT with a flexible window [2], as shown in Fig. 7(a)–(i), allows measurement of the frequency interval also in the presence of low SNR with errors of about 5%.

The above-mentioned results, therefore, highlight the excellent performance of (i) the Gabor representation together with the biorthogonal method in the computing of the coefficients $a_{m,n}$, (ii) the WVD, and (iii) the SCZT with a flexible window, in the detection of echoes to measure thickness in thin multilayer structures.

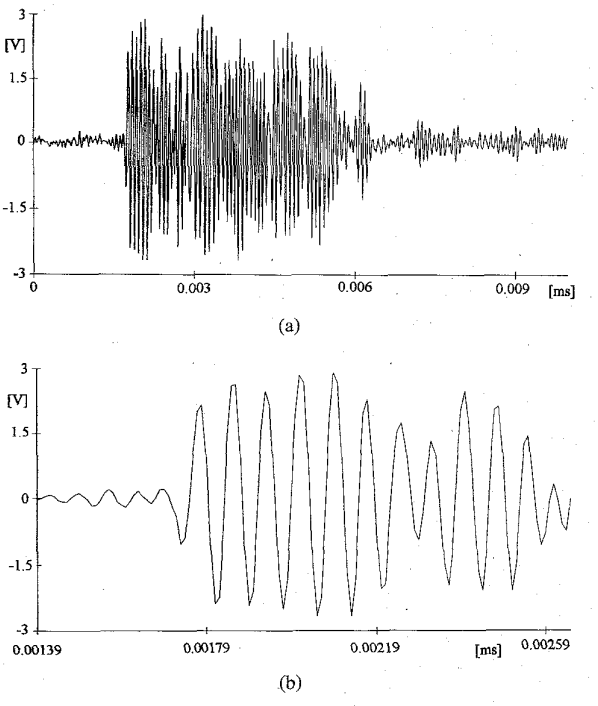

Fig. 8. (a) Real echographic signal, and (b) retina-choroid area.

B. Tests on Real Signals

After the initial emulation phase, the algorithms, optimized in the previous phase, were applied to real ultrasonic signals, obtained from an ophthalmic echograph and digitized by a high-sampling-rate transient digitizer (100 MHz, 8 bits, 1024 points/frame) at the Institute of Ophthalmology of the University of Naples.

Fig. 8 shows, as an example, a signal from the retina/choroid area, while, Fig. 9 shows the results of the application of TFR's on this signal. In particular, the authors have carried out signal acquisition on 28 normal subjects (48 normal eyes) consisting of 17 men (29 eyes) and 11 women (19 eyes) between the ages of 18 and 81 years.

The results of TFR applications are reported in Table III. They are obtained with the STFT with the Hamming window, the WVD with the Hamming window, the Gabor expansion with the biorthogonal method ($\lambda = 1, L = 64, N = 16$) and with the Zak Transform, and the CAF.

It is clear that the STFT, the WVD and the Gabor expansion with the biorthogonal method and the Zak Transform are able to detect the retina and choroid thickness. The WVD and the Gabor expansion with the biorthogonal method detect these thicknesses with a low number of ambiguity cases. Furthermore, the CAF is not able to detect the retina and choroid thickness. Finally, the SCZT furnished only the retina thickness $(140 \pm 11)\mu$m [17].

IV. CONCLUSION

The use of dedicated algorithms proved to be essential for the analysis of noisy ultrasonic signals in the characterization of multilayer structures. A suitable emulation and measurement procedure was set up allowing the performance of the implemented algorithms to be analyzed and compared with traditional techniques.

The experimental analysis was carried out by first emulating signals with different SNR's and noise bandwidths. Traditional techniques fail when the SNR decreases ($S/N \approx 5$ dB), whereas the time-frequency signal analysis achieves satisfactory performances.

All the signal-processing techniques were then applied to an *in vivo* application, namely to signals coming from the posterior surfaces of the human eye, obtaining particularly satisfactory results in the use of the Wigner-Ville Distribution.

Outgoing activity is oriented to analyze both the influence of the chosen "analysis window" in the TFR behavior, and

Authorized licensed use limited to: Columbia University. Downloaded on February 8, 2009 at 20:43 from IEEE Xplore. Restrictions apply.

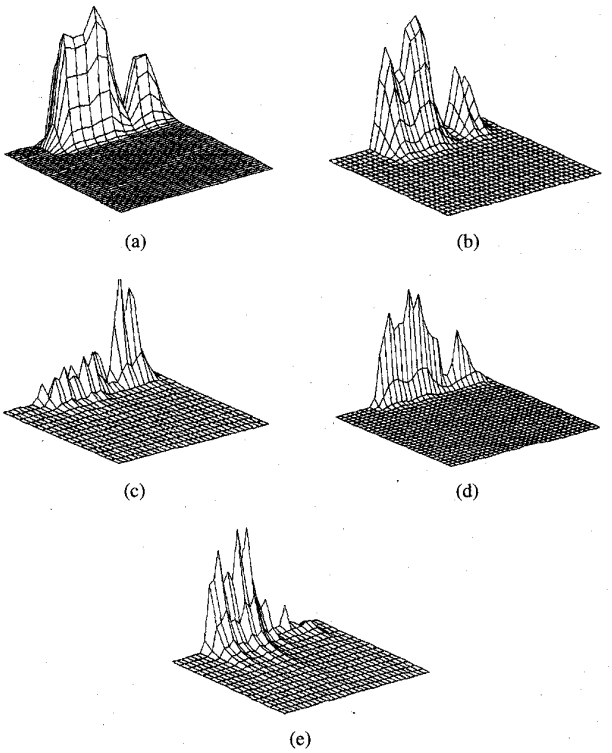

Fig. 9. Results obtained by using (a) the STFT, (b) the WVD, (c) the CAF, (d) the Gabor representation computing the coefficients $a_{m,n}$ by means of the biorthogonal method, and (e) the Gabor representation with the $a_{m,n}$ computed by Zak transform, applied to the real signal of Fig. 8(b).

interesting recent developments include the wavelet transform, the signal-adaptive WD smoothing, and so on.

ACKNOWLEDGMENT

The authors would like to thank the reviewers for their suggestions that improved the readability of this paper.

REFERENCES

[1] R. W. Schafer and L. R. Rabiner, "Digital representation of speech signals," *Proc. IEEE*, Apr. 1975, vol. P-63, pp. 662–677.
[2] G. Betta and P. Daponte, "Detection of echoes in noisy environments for multilayer structure characterization," *IEEE Trans. Instrum. Meas.*, vol. 42, no. 4, pp. 834–841, Aug. 1993.
[3] J. Ophir, Y. Yadzi, T. S. Lin and D. P. Shattuck, "Optimization of speed-of sound estimation from noisy ultrasonic signals," *IEEE Trans. Ultrason., Ferroelec. Freq. Contr.*, vol. 36, pp. 16–24, Jan. 1989.
[4] X. M. Lu, J. M. Reid, K. Soetanto, L. Weng and V. Genis, "Cepstrum technique for multilayer structure characterization," in *Proc. IEEE 1990 Ultrason. Symp.*, Honolulu, HI, 1990, pp. 1571–1574.
[5] V. K. Nair, K. Ludwig and R. F. Anastasi, "The Chirp-Z Transform applied to adhesively bonded structures," *IEEE Trans. Instrum. Meas.* vol. 40, pp. 751–759, Aug. 1991.
[6] D. J. Coleman and F. L. Lizzi, "In vivo choroidal thickness measurement," *Amer. J. Ophtalmology*, vol. 88, pp. 369–374, July 1979.
[7] H. Ohkawai *et al.*, "In vivo measurement of thickness or of speed of sound in biological tissue structures," *IEEE Trans. Sonics and Ultrason.*, vol. SU-30, pp. 231–237, July 1983.
[8] S. Tane *et al.*, "The microscopic biometry of the thickness of human retina, choroid and sclera by ultrasound," in *Proc. 10th SIDUO Cong.*, 1987, Sarasota, FL, W. Junke Publishers, pp. 131–136.
[9] F. Hlawatsch and G. F. Boundreaux-Bartels, "Linear and quadratic time-frequency signal representations," *IEEE Sig. Proc. Mag.*, pp. 21–57, Apr. 1992.
[10] L. Cohen, "A time-frequency distributions—A review," *Proc. IEEE*, July 1989, vol. 77, no. 7, pp. 941–981.
[11] B. Boashash, "Estimating and interpreting the istantaneous frequency of a signal—Part I: Fundamentals," *Proc. IEEE*, Apr. 1992, vol. 80, no. 4, pp. 520–538.
[12] B. Boashash, "Estimating and interpreting the istantaneous frequency of a signal—Part II: Algorithms and applications," *Proc. IEEE*, Apr. 1992, vol. 80, no. 4, pp. 540–568.
[13] D. J. Coleman, F. Lizzi and R. L. Jack, *Ultrasonography of the Eye and Orbit*, Philadelphia, PA: Lea & Febiger, 1977.
[14] P. Daponte and M. Savastano, "Noise problems in ophtalmic echography," in *Proc. of 1st IMEKO Symp. Meas. Elec. Quantities*, Como, Italy, June 1986, pp. 39–44.
[15] P. L. Carson, "What a hospital physicist needs in a transducer characterization standard: Are tissue-equivalent test objects necessary?," *IEEE Trans. Sonics Ultrason.*, vol. SU-26, pp. 1–7, Jan. 1979.
[16] W. Bushmann, W. Haigis and D. Linnert, "Influence of equipment parameters on results in ophtalmic ultrasonography," in *Proc. 8th SIDUO Cong.*, Nijmengen, The Netherlands, W. Junke, 1981, pp. 487–497.
[17] F. Cennamo, G. Cennamo and P. Daponte, "Ocular tissue characterization in vivo by RF signals analysis," in *Proc. 25th Int. Cong. Ophtalmology*, Rome, Italy, Kugler, 1986, pp. 231–237.
[18] J. B. Allen and L. R. Rabiner, "A unified approach to short-time Fourier analysis and synthesis," *Proc. IEEE*, Nov. 1977, vol. 65, no. 11, pp. 1558–1564.
[19] R. S. Orr, "The order of computation for finite discrete Gabor transforms," *IEEE Trans. Signal Processing*, vol. 41, no. 1, pp. 122–130, Jan. 1993.
[20] B. Friedlander and B. Porat, "Detection of transient signals by the Gabor representation," *IEEE Trans. on Acoust., Speech, Signal Processing*, vol. 37, no. 2, pp. 169–179, Feb. 1989.
[21] T. Genossar and M. Porat, "Can one evaluate the Gabor expansion using Gabor's iterative algorithm?," *IEEE Trans. Signal Processing*, vol. 40, no. 8, pp. 1852–1861, Aug. 1992.
[22] R. S. Orr, "Derivation of Gabor transform relations using Bessel's equality," *Signal Processing*, vol. 30, pp. 257–262, 1993.
[23] ——, "The order of computation for finite discrete Gabor transforms," *IEEE Trans. Signal Processing*, vol. 41, no. 1, pp. 122–130, Jan. 1993.
[24] S. Qian and D. Chen, "Discrete Gabor transform," *IEEE Trans. Signal Processing*, vol. 41, no. 7, pp. 2429–2438, July 1993.
[25] L. Auslander, I. C. Gertner and R. Tolimieri, "The discrete Zak transform application to time-frequency analysis and synthesis of nonstationary signals," *IEEE Trans. Signal Processing*, vol. 39, no. 4, pp. 825–835, Apr. 1991.
[26] A. J. E. M. Janssen, "The Zak transform and some counterexamples in time-frequency analysis," *IEEE Trans. Inform. Theory*, vol. 38, no. 1, pp. 168–171, Jan. 1992.
[27] L. Auslander and R. Tolimieri, "Computing decimated finite cross-ambiguity functions," *IEEE Trans. on Acoust., Speech, Signal Processing*, vol. 36, no. 3, pp. 359–364, Mar. 1988.
[28] E. Wigner, "On the quantum correction for thermodynamic equilibrium," *Phys. Rev.*, no. 40, pp. 749–759.
[29] J. Ville, "Theory and application of the notion of the complex signal," *Cables et Transmission*, no. 2, pp. 67–74. Translated to English by I. Salim, Rand Corp. Rept. T-92, Aug. 1, 1958.
[30] W. A. Gardner, "Statistical spectral analysis," Prentice-Hall, Englewood Cliffs, NJ, 1988.
[31] B. Boashash and P. J. Black, "An efficient real-time implementation of the Wigner-Ville distribution," *IEEE Trans. Acoust., Speech, Signal Processing*, vol. ASSP-35, no. 11, pp. 1611–1618, Nov. 1987.
[32] B. Boashash and P. O'Shea, "A methodology for detection and classification of some underwater acoustic signals using time-frequency analysis techniques," *IEEE Trans. Acoust, Speech, Signal Processing*, vol. 38, no. 11, pp. 1829–1841, Nov. 1990.
[33] G. Andria, E. D'Ambrosio, M. Savino and A. Trotta, "Application of Wigner-Ville distribution to measurements on transient signal," in *Proc. of IMTC'93*, Irvine (USA), May 1993, vol. 18–20, pp. 612–617.
[34] R. G. Baraniuk and D. L. Jones, "A signal-dependent time-frequency representation: Fast algorithm for optimal Kernel design," *IEEE Trans. Signal Processing*, vol. 42, no. 1, pp. 134–146, Jan. 1994.
[35] T. A. C. M. Claasen and W. F. G. Macklenbräuker, "The Wigner distribution—A tool for time-frequency analysis," *Philips J. Res.*, vol. 35, pp. 612–617, 1980.
[36] B. Boashash, "Note on the use of the Wigner distribution for time frequency signal analysis," *IEEE Trans. Acoust., Speech, Signal Processing*, vol. 36, no. 9, pp. 1518–1521, Sept. 1988.
[37] B. Zhang and S. Sato, "A time-frequency distribution of Cohen's class with a compound Kernel and its application to speech signal processing,"

Authorized licensed use limited to: Columbia University. Downloaded on February 8, 2009 at 20:43 from IEEE Xplore. Restrictions apply.